Determination of Watershed Infiltration and Erosion Parameters from Field Rainfall Simulation Analyses

Mark E. Grismer

Hydrologic Sciences and Biological & Agricultural Engineering, UC Davis, Davis, CA 95616, USA; megrismer@ucdavis.edu; Tel.: +1-530-304-5797

Abstract: Realistic modeling of infiltration, runoff and erosion processes from watersheds requires estimation of the effective hydraulic conductivity (K_m) of the hillslope soils and how it varies with soil tilth, depth and cover conditions. Field rainfall simulation (RS) plot studies provide an opportunity to assess the surface soil hydraulic and erodibility conditions, but a standardized interpretation and comparison of results of this kind from a wide variety of test conditions has been difficult. Here, we develop solutions to the combined set of time-to-ponding/runoff and Green–Ampt infiltration equations to determine K_m values from RS test plot results and compare them to the simpler calculation of steady rain minus runoff rates. Relating soil detachment rates to stream power, we also examine the determination of "erodibility" as the ratio thereof. Using data from over 400 RS plot studies across the Lake Tahoe Basin area that employ a wide range of rain rates across a range of soil slopes and conditions, we find that the K_m values can be determined from the combined infiltration equation for ~80% of the plot data and that the laminar flow form of stream power best described a constant "erodibility" across a range of volcanic skirun soil conditions. Moreover, definition of stream power based on laminar flows obviates the need for assumption of an arbitrary Mannings "n" value and the restriction to mild slopes (<10%). The infiltration equation based K_m values, though more variable, were on average equivalent to that determined from the simpler calculation of steady rain minus steady runoff rates from the RS plots. However, these K_m values were much smaller than those determined from other field test methods. Finally, we compare RS plot results from use of different rainfall simulators in the basin and demonstrate that despite the varying configurations and rain intensities, similar erodibilities were determined across a range of infiltration and runoff rates using the laminar form of the stream power equation.

Keywords: rainfall-runoff modeling; rainfall simulations; effective hydraulic conductivity; infiltration; laminar or turbulent flows; erodibility

1. Introduction

Modeling watershed runoff and erosion processes realistically requires field determination or model calibration estimation of surface soil infiltration rates or effective hydraulic conductivities (K_m) and erosion rates because they vary with soil cover/tilth/slope conditions, and seasonally with changing water contents. The field methods often used to measure in situ saturated or effective hydraulic conductivities (K_s or K_m, respectively, where K_m is some fraction of K_s) include surface (e.g., disk, single/double-ring infiltrometers, and rainfall simulators), or subsurface techniques (e.g., bore-hole methods). Indirect estimates of K_m and erodibilities available from NRCS soil survey information that are typically derived from soil texture information are also more often used in modeling than field measured values due to the difficulty associated with the field measurements and their variability. While each measurement method may have particular advantages depending on the intended use of the data, surface methods enable measurement of actual conditions as affected by soil

tilth and surface cover while also providing insights into the effectiveness of soil restoration methods in the field. However, they are not without complications associated with surface disturbance/roughness, type and configuration of surface cover, steep slope (double-ring methods require mild slopes), disk plate hydraulic contact and estimation from rainfall minus runoff rates using rainfall simulators. Similarly, subsurface measurement techniques or K_m estimation from soil texture information may miss the effect of surface layers on infiltration storage or excess leading to runoff–erosion prediction failure.

Here, we focus on determination of K_m and erodibilities from rainfall simulation (RS) methods in the field as these are not limited by surface conditions, slope or soil type. Following development of an integrated infiltration and time-to-ponding/runoff equation, we use infiltration and runoff data from over 425 RS plots in the Tahoe Basin, together with simultaneous measurements of saturated hydraulic conductivity, K_s, using bore-hole or mini-disc infiltrometers at selected sites to determine what estimation method of K_m yields the most consistent results. Then we consider the erosion process and soil detachment data from disturbed skirun soils to investigate the relationship between soil detachment and stream power to determine what form (laminar or turbulent) of the stream power function is most appropriate to describe overland sheet flows typical in RS test and forest soils. Finally, we consider test plot results from three different rainfall simulators used at similar locations to demonstrate application of the equations for determination of K_m and erodibilities associated with RS tests having a range of raindrop impact energies.

1.1. Brief Literature Review

Rainfall simulators (RSs) are essential tools for investigating the dynamic processes of infiltration, runoff and erosion under a variety of field conditions [1–4], and information from RS test plots can provide the infiltration/runoff parameterization required for watershed modeling. Though multiple RS designs for field application exist, no single RS design (including plot runoff frame installation) has emerged as a standard. Similarly, while in RS plot tests, typically, data about rainfall, runoff and erosion rates and time to runoff are collected from which infiltration rates, or K_m and erodibilities are estimated, no standard RS data analysis methodology has evolved. Despite a number of years of research into the plant/cover effects on soil erosion [5–12], it remains difficult to understand erosion processes and mechanics due to the lack of sufficiently comparable data or results [8,13]. Moreover, the differences in soil properties, slope surface conditions and vegetation types in field experiments have tended to complicate interpretations of field measurements. It is difficult, therefore, to draw meaningful comparisons between RS plot data reported in different studies [2–4,14,15]. In addition, there are few, if any, actual comparisons of RS performance with respect to infiltration, erosion, or soil detachment rates. For example, Lascelles et al. [16] only considered the variability in drop sizes, distributions and energies from two different RSs and speculated on implications with respect to erosion, but did not offer comparison RS plot studies. Similarly, Kinnell [17,18] completed thorough reviews of the processes associated with raindrop impacted erosion and noted that both conceptual models and measurements fail in various respects to adequately characterize field observed erosion processes from bare soils. Concerns such as these have also arisen in the Tahoe Basin, because a variety of methods for measurement of infiltration and erosion rates have been deployed, but comparisons between results of different studies remain less than definitive.

1.2. Project Hypothesis & Objectives

Data from RS field plots can be used to assess the initiation time of runoff, an indication of surface conditions (though, admittedly, from perhaps unusually large rainfall rates, or associated durations), the subsurface infiltration characteristics through determination of the infiltrated volume after a RS test time, as well as soil detachment rates or "erodibilities". In order to develop more widely usable information/data, standardized approaches to the RS plot setups and the subsequent data analyses are needed [2]; here we focus on the latter, using RS test data from 425 plots across the Lake Tahoe Basin. We hypothesize that there exists a physically consistent set of equations that relate infiltration

and erosion data collected from different RS test plots to surface soil effective hydraulic conductivity and erodibility. The primary project objectives include: (a) develop the appropriate infiltration and erosion equations applicable to field RS plots, (b) evaluate the applicability of these equations to a large RS data set, and (c) use these equations to compare RS test plot results from three different field rainfall simulators having a range of rain drop energies and rainfall configurations to both demonstrate their applicability and determine whether differences in raindrop impact energy result in significantly different K_m values or erodibilities for the Tahoe Basin soils.

1.3. Theory—Infiltration Equation Development

Several infiltration equations have been derived during the past few decades and the most often used in watershed modeling revolve around time-to-ponding estimates and the ponded infiltration Green–Ampt type square-wave wetting-front formulation, among others. In RS plot studies, the applied rainfall rates are generally large and for durations that exceed that of natural rainfall so as to achieve runoff after some acceptable elapsed time after rainfall initiation. As such, there are typically a few minutes during which the plot infiltration capacity exceeds that of the applied rainfall followed by shallow ponded infiltration. Ideally, the effective hydraulic conductivity that satisfies both the time-to-ponding and ponded infiltration equations would represent the self-consistent field value that then should apply in watershed modeling. We briefly define terms and develop these equations here, eventually coupling the ponding time and Green–Ampt–type equations to allow implicit determination of K_m from the RS data outlined above.

Basic definitions from Grismer [19] include:

$$h_e \;=\; \frac{h_d}{h_c} \tag{1}$$

where h_d = displacement pressure head (mm), and h_c = capillary pressure head (mm)

$$S_e = \frac{S - S_r}{S_m - S_r} \;\cong\; h_e{}^\lambda \tag{2}$$

where S = saturation, S_r = residual saturation, S_m= maximum saturation associated with infiltration, and λ = pore-size distribution index.

And the Green–Ampt infiltration equation takes the form

$$I \;=\; K_m(H \,+\, h_f \,+\, z_f)/z_f \tag{3}$$

where I = infiltration rate (mm/hr),

K_m = "natural saturated hydraulic conductivity" (mm/hr) $\approx 0.5 K_s$,
H= ponding depth (mm),
h_f = wetting front capillary pressure head (mm), and
z_f = wetting front depth (mm).

Combining the Green–Ampt Equation (3) with the continuity equation yields

$$t = \frac{1}{K_m}\left\{ V - \phi\left(S_m - S_i\right)\left(H \,+\, h_f\right)\ln\left[1 + \frac{V}{\varphi\left(S_m - S_i\right)\left(H + h_f\right)}\right]\right\} \tag{4}$$

where V = volume infiltrated per unit area (mm).

The Green–Ampt equation above is readily modified to account for air resistance to wetting flow by using β to replace the 1 at the beginning of the RHS of Equation (4) and h_f within the parentheses with H_c [19]. β and H_c are defined as follows

$$\beta = \frac{1}{\mu_w} \int_1^{S_e} \frac{d^2 f_w / dS_e^2}{\left[(k_{rg}/\mu_g) + (k_{rw}/\mu_w) \right]} \, dS_e \tag{5}$$

where μ_w and μ_g are the water and air viscosities, respectively, similalry k_{rw} and k_{rg} are the relative permeabilities of the porous media to water and air, respectively. S_e is the effective saturation and f_w is the fractional flow function of water, or the ratio of water flow to total (air and water) flowrate. For all practical purposes, β takes on a value between 1.2 and 1.3 for typical λ values between 2 and 3, an index range that covers loamy to sandy soils [19]. The wetting front driving head, H_c can be determined from

$$H_c = h_d \int_1^{h_e} \frac{f_w}{h_e^2} \, dh_e \tag{6}$$

where h_e is defined in Equation (1). Again for all practical purposes, H_c takes on a value between 1.12 h_d – 1.08 h_d for λ between 2 and 3. Substituting Equations (5) and (6) in the Green–Ampt Equation (4) to correct for air resistance or counterflow during infiltration results in [19]

$$t = \frac{\beta}{K_m} \left\{ V - \phi \left(S_m - S_i \right) \left(H + H_c \right) \ln \left[1 + \frac{V}{\varphi \left(S_m - S_i \right) \left(H + H_c \right)} \right] \right\} \tag{7}$$

Finally, the corresponding 'time–to-ponding' infiltration equation that accounts for air resistance or counterflow as well is given by

$$t_p = \frac{\varphi \left(S_m - S_i \right)}{(1 - f_w) q_o} H_c \exp \left[\left(\frac{q_o \beta}{K_m} - 1 \right)^{-1} - 1 \right] \tag{8}$$

where q_o is the rainfall rate and f_w is practically zero for ponded infiltration (see Morel-Seytoux [20] discussion linking the transition of rainfall rate controlled infiltration conditions to that for ponded infiltration).

With a relationship between h_d and K_m together with the time-to-ponding, infiltrated depth and times from RS plot data, Equations (7) and (8) can be solved simultaneously for K_m (assuming that $K_m = 0.5 K_s$) by solving Equation (8) for $\varphi(S_m - S_i)$ and letting $f_{wi} = 0$. Using lab column data collected to date, Grismer [19] determined that for h_d in meters, the semi-empirical theoretical relationship for permeability was k (μm^2) $\approx 0.84/h_d^2$. Using only that lab data for sands that more closely replicate the Tahoe soils and changing to more directly applicable units, we found that K_m (mm/hr) = 19.9/$h_d^{2.4}$ for h_d (mm), as shown in Figure 1. And as noted above, taking $H_c \cong 1.1 h_d$, $\beta \cong 1.3$ for λ = 3, and the ponded depth H of Equations (4) or (7) as typically assumed to be small (e.g., 1 mm as in watershed modeling, [21]), we can implicitly solve for K_m from Equations (7) and (8) by re-arranging Equation (8) to solve for $\Delta\theta = \varphi(S_m - S_i)$, as shown below as Equation (9) and substituted into Equation (7).

$$\Delta\theta = \frac{(q_o t_p / H_c)}{\exp \left[\left(\frac{\beta q_o}{K_m} - 1 \right)^{-1} - 1 \right]} \tag{9}$$

Alternatively, we can use the simpler Main–Larson equations analogous to Equations (7) and (9) below, but still accounting for air-resistance to infiltration

$$t_p = \frac{\varphi \left(S_m - S_i \right) H_c}{q_o \left(\frac{q_o}{K_m} - 1 \right)} \tag{10}$$

and

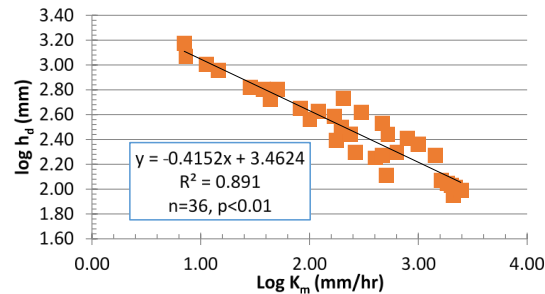$$\Delta\theta = \left(\frac{q_o\, t_p}{H_c}\right)\left(\frac{q_o}{K_m} - 1\right)$$　　(11)

Figure 1. Relationship between field-saturated hydraulic conductivity, K_m, and displacement pressure head, h_d, for fine sands (data taken from Grismer, [19]).

Finally, we can use the estimated effective $\Delta\theta$, taken as the measured infiltrated depth compared to the visual wetting front depth, from RS plot data when no runoff occurs, combined with the infiltrated depth and RS test duration to determine K_m from Equation (7). For example, Figure 2 shows the relationship between visual wetting and infiltrated depths from the long-term monitoring site at Heavenly ski area on the coarser-textured granitic soils where the average regression slope suggests an effective $\Delta\theta \cong 45\%$.
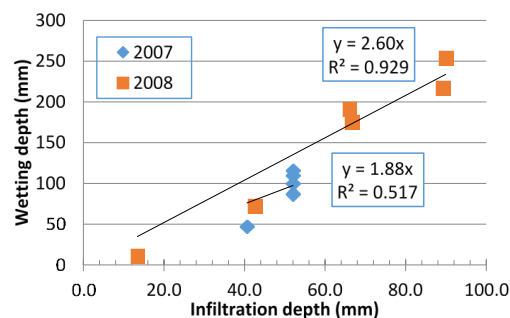

Figure 2. RS (rainfall simulation) plot infiltrated vs. visible wetting depths at Heavenly LT site (granitic soils).

1.4. Theory—Erosion Equation Development

Most watershed modeling efforts and associated estimation of sediment detachment or erosion rates employ the well-known Manning's equation to relate overland or channel flowrates and velocity to flow depth and hillslope, or channel gradient. Of course, use of Manning's equation implies that an appropriate surface roughness value, "n", can be identified, that the driving force, or slope angle <10% and that flows are fully turbulent. The assumption of turbulent flow conditions during sheet flow across the RS plot or the landscape is questionable when flow depths are quite small and laminar flows are more likely present [21]. The general derivation of the laminar flow equation for thin films on inclined planes at any angle, α, to the horizontal requires only the assumptions of the "no-slip" boundary condition together with constant fluid properties [22]. Considering two-dimensional steady laminar flow of depth, y, down an inclined plane at angle, α, to the horizontal, the shear force as given by the fluid viscosity, μ, and the parabolic velocity function is balanced by the gravitational force (unit weight, ρg) on the fluid body in the direction of flow. That is, the flowrate Q per unit width is given by

$$Q = u_m\, y = (\rho g y^3/3\mu)\sin\alpha$$　　(12)

where u_m is the mean velocity taken as $2/3^{rds}$ of the maximum velocity assuming a parabolic velocity distribution perpendicular to the inclined plane. Of course, the equivalent flowrate equation assuming turbulent flow and mild slopes (<10%) is taken from the approximation for the Chezy–Mannings equation assuming flow depths are very small compared to flow width, B,

$$Q \ = \ (1/n)\,y^{1.67}S^{0.5} \tag{13}$$

The flow mean velocity needed to determine shear stresses on soil particles is given by Q/y from Equations (12) or (13), depending on whether laminar or turbulent flow is assumed. Replacing the sine function with a power function approximation in Equation (14), it is apparent that under steady laminar flow conditions the mean surface flow velocity is practically proportional to the slope, S, rather than the square root of the slope, as in the mean velocity determined from Manning's Equation (15); moreover, there is no slope limitation or need to identify the roughness value, "n".

$$u_m \ = \ (\rho g y^2/3\mu)\sin\alpha \cong (0.7524\,\rho g y^2/3\mu)S^{0.983} \tag{14}$$

$$u_m \ = \ (1/n)\,y^{0.67}S^{0.5} \tag{15}$$

In RS plot studies, the runoff rate, q, is often expressed as the steady flowrate collected at the runoff lip frame divided by the area of the plot, as this allows convenient comparison to the infiltration and rainfall rates, and because rarely is the actual sheet flow depth measured or estimated so as to enable calculation of the mean, or average, overland flow velocity, u_m. The relationship between q and u_m is simply given by the mass balance

$$q \ = \ By u_m/A, \ \text{or} \ u_m \ = \ qA/(By) \tag{16}$$

where A = runoff frame area (m^2), B = the runoff lip width (m) and the other parameters are as previously defined. Solving Equation (16) for the mean velocity then requires substitution for the flow depth based on either Equation (15) for turbulent flow, or Equation (14) for laminar flow, as shown below, respectively, in Equations (17) and (18).

$$u_m \ = \ (qA/B)^{0.4}\,S^{0.3}/n^{0.6} \ = \ \left(\frac{A}{Bn^{1.5}}\right)q^{0.4}s^{0.3} \tag{17}$$

$$u_m \ = \ (qA/B)^{0.67}\,(0.7524\rho g/3\mu)^{0.33}\,S^{0.328} \ = \ \left(\frac{A}{B}\right)^{0.67}\left(\frac{0.25\rho g}{\mu}\right)^{0.33}q^{0.67}S^{0.328} \tag{18}$$

Quantitative description of soil particle detachment or erosion processes perhaps originated with Ellison's [23] observation that "erosion is a process of detachment and transport of soil materials by erosive agents". These "erosive agents", of course, include raindrop impact and overland flow. Of course, rain drop impact energy diminishes with increasing flow depth and presence of soil cover that both "absorb" the drop impact energy. Raindrop impact energy, while an erosive agent on bare soils should probably be related to the aggregate strength, that is, the energy needed to break up and mobilize surface aggregates [24,25]. Subsequent research, more or less, begins with Ellison's paradigm of sorts that continues in concept through the soil-detachment equation review by Owoputi and Stolte [26]. Similarly, Foster and Meyer [27] interpreted results of several experiments in terms of Yalin's equation that assumes "sediment motion begins when the lift force of flow exceeds a critical force . . . necessary to . . . carry the particle downstream until the particle weight forces it out the flow and back to the bed." Bridge and Dominic [28] built on this concept and described the critical velocities and shears needed for single particle transport over fixed rough planar beds. Gilley et al. [29–31] included the Darcy–Weisbach friction factor as a measure of the resistance to flow that was eventually adopted in the WEPP model. Moore and Birch [32] combined slope and velocity and suggested that particle transport and transport capacity for both sheet (interrill) and rill flows is best derived from the

unit stream power. In all these descriptions, the erodibility process essentially involves momentum transfer with an energy loss to friction. More recently, the concept of stream power as the primary factor controlling soil detachment rates has been adopted in several reviews e.g., [33–36]. Assuming turbulent and laminar flow conditions, respectively, from Equations (17) and (18), stream power, P, can be expressed as

$$P = \rho g u_m S = \left(\frac{A}{Bn^{1.5}}\right)^{0.4} \rho g q^{0.4} S^{1.30} \tag{19}$$

and

$$P = \left(\frac{A}{B}\right)^{0.67} \left(\frac{0.251}{\mu}\right)^{0.33} (\rho g)^{1.33} q^{0.67} S^{1.328} \tag{20}$$

Note that in both Equations (19) and (20), slope, S, has a practically the same effect on stream power, hence detachment rate, whether the flow is laminar or turbulent; that is, P is proportional to $S \sim^{1.3}$. However, the runoff rate under laminar flow conditions has a much greater affect than that under turbulent flow conditions (i.e., P is proportional to $q^{0.67}$ as compared to $q^{0.4}$), as do the unit weight and plot dimensions (though offset to some degree by 'n'). Nonetheless, in terms of practical analyses of RS plot runoff and erosion data, when rain splash impacts are negligible, it is apparent that the soil particle detachment rate is proportional to $\sim S^{1.3}$ and q^a, where 'a' takes on a value between 0.4 and 0.7.

Experimentally, the dependence of stream power on slope between laminar and turbulent flow is not well articulated. In fact, at slopes of 4%–12%, McCool et al. [37] found soil loss rates dependent on $S^{1.37}$–$S^{1.5}$, rather than $S \sim^{1.3}$. In flume studies, Zhang et al. [38] found across a slope range of 3%–47% their detachment data was proportional to $q^{2.04} S^{1.27}$ suggesting that both Equations (19) and (20) may underestimate the effects of runoff rate. At small slopes, detachment rate was more sensitive to q than S, however, as S increased, its influence on detachment rate increased. Later, Zhang et al. [39] found that for undisturbed "natural" soils across a similar slope range (9%–47%), detachment rates were most proportional to $q^{0.89} S^{1.02}$. In contrast, on nearly flat slopes (1%–2%) with deep flow depths (~10 mm), Nearing and Parker [40] found that turbulent flow resulted in far greater soil detachment rates than did laminar flow, in part as a result of greater shear stresses. Following Gilley and Finkner [29], Guy et al. [41] examined the effects of raindrop impact on interrill sediment transport capacity in flume studies at 9%–20% slopes. Assuming a laminar flow regime, they found that raindrop splash accounted for ~85% of the transport capacity, in some contrast to earlier studies indicating that raindrop impact had little or no effect on slopes greater than about 10%. Sharma et al. [42–44] systematically examined rain splash effects on aggregate breakdown and particle transport in the laboratory but did not relate their results to stream power. At larger slopes, Lei et al. [45] found that both slope and runoff rate were important towards transport capacity on slopes up to about 44%, but that transport capacity increased only slightly at still steeper slopes. Zhang et al. [39] found the best linear regression quantifying soil detachment rates occurred for equations that included the square of the rainfall rate (I^2) times the WEPP slope factor, or I times the runoff rate and slope, S, as compared to I times the square root of the runoff rate times $S^{0.67}$. This observation of a better fit with the first two equations suggested that detachment rate is proportional to stream power. Similarly, considering soil detachment from overland flow only across a range of burned, disturbed and relatively undisturbed rangeland soils with slopes of 6%–57%, Al-Hamdan et al. [35] found that detachment rates were proportional to $P^{1.18}$, but that the exponent of 1.18 did not differ significantly from unity. Gabriels [34] found that detachment rates were related to $P^{1.3}$ for a range of clay fractions of 7%–41%, an exponent value consistent with that for the plot slope in Equations (19) and (20). In the RS plot studies considered here, we assume that detachment rates are proportional to $S \sim^{1.3}$ and then determine the optimal exponent applicable to the runoff rate.

2. Experimental Methods—Infiltration–Runoff and Hydraulic Conductivity Measurements in the Field

In the analyses here, we use field data collected from 423 RS plots and associated measurements of hydraulic conductivity for which overviews of the methodologies and some results were described elsewhere [46–51]. While most of the Lake Tahoe Basin (See Figure 3) soils are of andesitic or granitic origin and of sandy textures from soil surveys (Table 1), we have found that the surface soils can be broadly classified as coarser-textured "granitics" and finer-textured "volcanics" (Table 2). In addition to the 1 m and 3 m tall drop-former (DF) type RSs used here, we also include information from the USDA-FS sprinkler RS described by Foltz et al. [52]. Table 3 summarizes the field methods and associated references used here to develop the data set considered in the infiltration and soil detachment analyses. The MDI and Precision permeameter methods both involved repeated measurements (5–10 times per hole, or MDI test) and the bore-holes used varied from 150 to 300 mm deep and 70 mm in diameter, with a static water depth of 100–120 mm.

Table 1. Typical Tahoe soils encountered in the field measurements [53].

RS Sites	Soil Series	Taxonomic Classification	Surface Texture	pH	Conductivity (mm/h)
Bliss SP & Rubicon—granitic	Meeks	Sandy-skeletal, mixed, frigid Humic Dystroxerepts	very stony loamy coarse sand	6.1–6.5	16–51
Blackwood Cyn—volcanic	Waca	Medial-skeletal, amorphic, frigid Humic Vitrixerands	cobbly coarse sandy loam	5.6–6.5	5.1–16
Brockway & Dollar Hill—volcanic	Jorge-Tahoma	Fine-loamy, isotic, frigid Ultic or amorphic, frigid Ultic Haploxeralfs	very stony sandy loam	5.1–6.0	5.1–16

Table 2. Summary of sieved particle-size distribution measurements for the Tahoe Basin disturbed soils (>63 μm size fraction) and estimated K_{sat} values. From Grismer and Hogan [46].

Soil Type	n	D_{10} (μm)	D_{30} (μm)	D_{60} (μm)	[a] C_u	[b] K_{sat} (mm/hr)
Granitic—mean	33	117.1	322.5	946.4	8.23	332
Std. Deviation ([c] *CV* %)	33	20.4 (17.4)	73.9 (22.9)	208 (22.0)	1.96 (23.8)	116 (34.8)
Volcanic—mean	56	100	278	1320	13.6	248
Std. Deviation (*CV* %)	56	23.2 (23.2)	120 (43.3)	568 (48.5)	6.58 (53.1)	125 (50.4)

[a] C_u is the Coefficient of Uniformity = D_{60}/D_{10}; in geotechnical engineering, $C_u > 4$ indicates "well-graded" (i.e., broad range) of particles sizes; [b] K_{sat} = (Constant)xD_{10}^2 from Harleman et al. [53]; [c] *CV* = Standard Deviation/Mean.

Table 3. Summary of field measurement methodologies used to develop the datasets considered in the infiltration, soil detachment and RS comparisons analyses.

| Device/Method	Description	Parameters Measured	Reference
1 m Tall Drop–Former RS (~21% of terminal velocity raindrops)	1 m² Needle tank RS raining on 0.8 × 0.8 m² plot	Rain rate, wetting depth, soil moisture, time-to-ponding, runoff rate, runoff particle size distributions and sediment & OM concentrations	Grismer & Hogan [46]
3 m Tall Drop–Former RS (~70% of terminal velocity raindrops)	1 m² Needle tank RS raining on 0.8 × 0.8 m² plot	Rain rate, surface roughness, time-to-ponding, runoff rate, runoff sediment concentrations	Battany & Grismer [14,15] Grismer & Hogan [46]
Modified Purdue sprinkler RS (USDA–FS)	Single oscillating VeeJet nozzle RS raining on 1 m² plot	Rain rate, time-to-ponding, runoff rate, runoff sediment concentrations	Foltz et al. [52]
Decagon Mini-Disk Infiltrometer (MDI)	Surface infiltrometer with ceramic disk	Saturated conductivity (K_s) with & without surfactants	Robichaud et al. [54] Rice & Grismer [51]
Precision Permeameter	Bore-hole method using mariotte siphon on graduated cylinder	Saturated conductivity (K_s) of near surface soils	Johnson [55] Glover solution in Zanger [56]
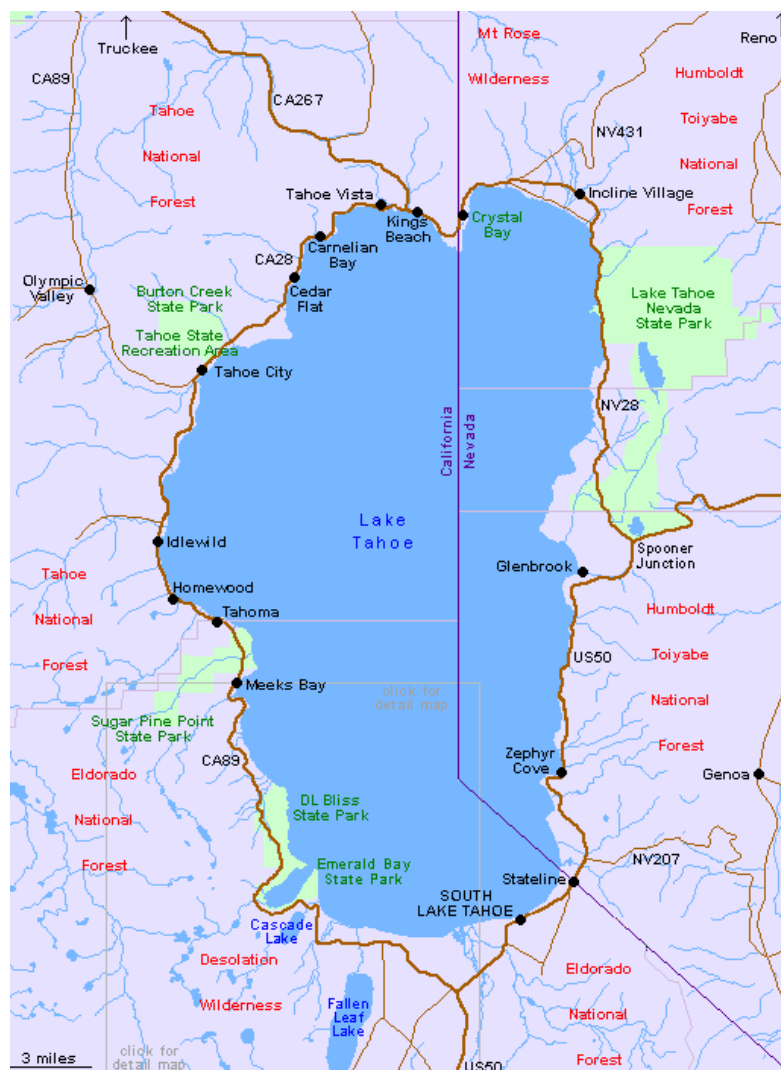
Figure 3. Lake Tahoe basin map (http://www.americansouthwest.net).

3. Results

3.1. Infiltration–Runoff Field Data

Tables 4 and 5 summarize the average RS plot characteristics for the granitic plots that both resulted in runoff, or not during the 30–60 min RS tests in the Tahoe Basin, respectively. Similarly, Tables 6 and 7 summarize the average RS plot characteristics for the volcanic plots that both resulted in runoff, or not during the RS test, respectively. Tables 4 and 5 also distinguish between non-hydrophobic and hydrophobic RS plot tests within the granitic soils. These data provide a unique opportunity to evaluate application of the combined Infiltration Equations (7) and (8) across a broad range of plot characteristics, such as initial soil moistures ranging from 2% to 12%, rainfall rates from 60–120 mm/h, RS test durations of 10–70 min, plot slopes from 6% to 72% and ponding times from 1–20 min. Also included in this analysis, were RS test plots having clearly identified hydrophobic surface soils; these plots always resulted in quite large Δθ values. In most cases, the infiltrated depths were obtained at the end of the RS test associated with the infiltrated time to be used in Equation (7).

Table 4. Summary of RS plot setting data averages for granitic soil plots generating runoff.

Granite Soil Site Descriptions—Non-Hydrophobic Plots	*n*	Rain Rates (mm/h)	Initial Moisture (%)	Average Slope (%)	Mean Time to Runoff (min)	Infilt Depth (mm)	Infilt Time (min)	Mean Δθ	St.Dev. Δθ
Bliss SP RC—bare	4	60	ND	64.3	3.5	13.68	15	ND	NA
Bliss SP RC—treated	3	60	ND	57.5	14	14.8	15	ND	NA
CalTrans BS Plots	3	72–120	ND	30.2	10.9	28.9	18.0	ND	NA
Cave Rock/Incline Village RC	10	60	2.3	59.2	7.0	35.7	37.8	0.20	0.13
Heavenly CAN LT—2005	4	72–120	2.3	16.9	5.3	45.3	30.0	ND	NA
Heavenly CAN LT—2006	1	120	ND	17.1	5.7	25.8	30.0	0.49	NA
Heavenly CAN LT—2007	6	72–120	ND	18.1	2.9	61.3	30.0	0.42	0.10
Heavenly GB MSR & OLB	17	120	4.0	25.3	8.1	69.9	36.2	0.36	0.16
Heavenly LRR	6	120	4.2	25.8	6.6	90.7	46.5	ND	NA
Heavenly LT—2006	3	72–90	2.4	22.9	3.2	37.5	28.3	ND	NA
Heavenly PON/MCD	5	72–120	4.2	23.5	4.6	27.3	23.0	0.41	0.16
Heavenly STC	5	120	4.4	35.8	3.4	39.5	21.5	0.93	0.23
Luther Pass RC	12	60	ND	51.5	2.64	12.4	15	ND	NA
Mammoth	7	120	4.8	34.9	7.1	50.7	27.7	0.30	0.14
Meyers RC	7	72–120	2.3	30.0	3.9	81.8	22.0	ND	NA
Roundhill landing	5	65–70	1.0	6.2	6.9	33.6	52.9	0.38	0.14
Roundhill landing—USFS	4	86	1.0	15.6	3.0	26.2	60.0	ND	NA
Rubicon RC, treated & native	12	60	ND	49.3	10.3	14.2	15.0	ND	NA
Truckee Bypass	6	72–120	1.0	26.2	16.3	44.5	31.1	0.37	0.09
Upper Cutthroat 1D & 2T	7	72–90	2.7	6.0	6.5	30.8	22.6	0.28	0.04
Upper Cutthroat 3T	4	120	2.7	5.1	17.7	89.9	46.1	0.54	0.33
Upper Cutthroat 4T & 6T	4	120	6.6	9.8	19.4	78.7	43.7	0.63	0.34
Upper Cutthroat 7T	3	120	2.0	7.3	5.1	36.9	25.9	0.37	0.09
Upper Cutthroat 8T	6	120	6.3	12.7	4.8	33.8	21.5	0.23	0.09
Angora Fire	8	72	ND	17.6	8.2	25.5	20.3	1.19	0.35
Bliss SP & Meyers RC—water	6	120	2.4	12.7	2.5	91.0	60.0	6.23	4.32
Heavenly LT—Natives—2006	3	72	2.2	27.3	1.4	6.8	8.6	ND	NA
Upper Cut. 10T & 11T	3	120	4.4	6.4	14.3	110.0	55.8	1.28	0.69
Upper Cut. 3N—natives	4	72–120	4.8	4.8	1.3	9.9	22.2	1.12	0.70

ND = No Data and NA = Not Applicable.

Table 5. Summary of RS plot setting data averages for granitic soil plots not generating runoff.

	n	Rain Rates (mm/h)	Initial Moisture (%)	Avg. Slope (%)	Infilt Depth (mm)	Infilt Time (min)	Mean Δθ	St.Dev. Δθ
Granite Soil Site Descriptions—Non-Hydrophobic Plots								
CalTrans OP Plots	3	72–120	ND	37.4	52.3	30.0	ND	NA
Cave Rock–Inc. Village RCs	4	60	1.29	53.1	30.0	30.0	0.59	NA
Heavenly CAN LT	10	72–120	1.70	14.9	82.4	39.3	ND	NA
Heavenly CAN LT	13	72–120	ND	17.9	102.9	51.4	0.43	0.11
Heavenly GB MSR & OLB	1	120	3.56	34.7	92.0	46.0	ND	NA
Heavenly STC	1	120	4.0	27.8	90.0	45.0	0.39	NA
Mammoth	2	120	4.39	38.4	90.0	45.0	0.59	0.08
Meyers RC	4	90–120	2.5	28.7	48.8	30.0	ND	NA
Roundhill landing	1	55	1.0	6.7	50.4	55.0	0.25	NA
Truckee Bypass	9	72–120	2.7	28.5	57.3	30.0	0.27	0.07
Upper Cutthroat 3T	2	72	5.38	6.8	69.8	58.2	0.47	0.05
Upper Cutthroat 4T & 6T	1	120	5.6	5.9	90.0	45.0	0.80	NA
Upper Cutthroat 8T	4	120	5.77	9.6	105.6	58.6	0.53	0.28
Granite Soil Site Descriptions—Hydrophobic plots								
Bliss SP & Meyers RC—surfactant	6	120	2.60	12.6	120.0	60.0	0.82	0.30
Angora Fire	1	72	ND	21.3	72.0	60.0	1.29	NA
Upper Cut. 10T & 11T	6	120	5.05	7.5	76.8	38.4	1.50	0.59

ND = No Data and NA = Not Applicable.

Table 6. Summary of RS plot setting data averages for volcanic soil plots generating runoff.

Volcanic Soil Site Descriptions	*n*	Rain Rates (mm/h)	Initial Moisture (%)	Average Slope (%)	Mean Time to Runoff (min)	Infilt Depth (mm)	Infilt Time (min)	Mean Δθ	St.Dev. Δθ
Blackwood Canyon–Truckee (hydrophobic)	8	120	1.89	12.5	18.2	105.9	60.0	0.68	0.16
Brockway Summit—2006	1	72	9.50	42.1	18.2	35.0	30.8	0.40	NA
Brockway Summit—2003	6	60	ND	51.0	3.5	12.3	15	ND	NA
Dollar Hill—Tall RS	4	61	11.46	52.2	4.15	13.83	15	ND	NA
Homewood #31 Rd	4	72	5.5	18.5	4.8	25.3	22.7	0.24	0.03

Table 6. *Cont.*

Volcanic Soil Site Descriptions	n	Rain Rates (mm/h)	Initial Moisture (%)	Average Slope (%)	Mean Time to Runoff (min)	Infilt Depth (mm)	Infilt Time (min)	Mean Δθ	St.Dev. Δθ
Homewood LL A&B Rd	6	120	5.0	37.5	5.1	43.0	22.8	0.26	0.02
Homewood MAR Rd	9	120	3.00	30.7	3.6	33.5	18.8	0.28	0.13
Homewood SCD RD&BK Rd	9	120	5.3	28.5	5.0	43.8	20.4	0.32	0.09
Homewood WDG Rd	8	120	9.9	22.5	3.2	17.5	9.8	0.40	0.19
Northstar—small RS	2	60	4.75	49.2	8.0	24.2	26.5	0.25	NA
Juniper Mtn Skirun	5	60–75	4.20	36.4	4.4	15.4	15.8	0.47	0.07
Juniper Mtn Skirun—WCs	3	100–125	8.67	35.4	9.3	41.0	22.8	1.58	0.40
Northstar—Tall RS	7	60	7.6	53.3	5.6	21.1	21.6	0.20	0.04
Northstar—bare ski Tall RS	13	60	NA	35.8	5.2	14.1	16.8	0.23	0.06
Homewood—Tall RS	18	60	3.7	42.5	9.6	19.5	22.4	0.14	0.13
Northstar BP CON plots	2	120	3.95	19.4	17.4	79.6	40.8	0.36	NA
Northstar LT	12	72–120	2.9	34.4	8.5	35.6	23.8	ND	NA
Northstar STA plots	3	120	5.3	42.6	2.7	23.1	12.6	0.48	0.06
Northstar Unit 7	2	120	3.75	39.7	4.4	44.8	23.8	ND	NA
Ward Cr. Landing—IERS	4	70	10.0	7.4	6.4	38.3	44.2	0.49	0.15
Ward Cr. Landing—USFS	3	91	10.0	18.1	2.1	26.1	60.0	ND	NA

ND = No Data and NA = Not Applicable.

Table 7. Summary of RS plot setting data averages for volcanic soil plots not generating runoff.

Volcanic Soil Site Descriptions–	n	Rain Rates (mm/h)	Initial Moisture (%)	Mean Slope (%)	Infilt Depth (mm)	Infilt Time (min)	Mean Δθ	St.Dev. Δθ
Blackwood–Truckee (Surf)	4	120	1.70	12.5	120.0	60.0	0.62	0.21
Brockway Summit plots	5	120	2.21	45.6	51.2	26.7	0.34	0.01
Northstar—Short RS	5	60	6.9	53.2	30.8	29.5	0.48	0.18
Northstar—Tall RS	7	60	8.9	55.7	39.6	38.2	0.30	0.08
Homewood—Tall RS	2	60	ND	20.9	41.0	41.0	0.12	NA
Juniper Mtn Skirun	16	60–125	7.46	38.7	42.4	30.0	ND	NA
Northstar BTD & BP CON	4	120	2.61	19.6	90.0	45.0	0.34	0.03
Northstar LT	6	72–120	2.3	32.4	44.0	30.0	ND	NA
Northstar Unit 7—Short RS	9	75–120	3.81	40.6	54.3	30.0	ND	NA

ND = No Data and NA = Not Applicable.

Finally, Table 8 lists the results of the saturated hydraulic conductivity, K_s measurements completed using the mini-disk infiltrometer (MDI) and Precision Permeameter (PP) devices at the various RS sites around the Tahoe Basin. The two K_s measurement methods yielded very similar results, in general, the average non-hydrophobic K_s values were 970 and 870 mm/h, respectively, for the granitic and volcanic soils, while the hydrophobic MDI K_s values were roughly 10%–40% of the non-hydrophobic values. The measured K_s values are 3–4 times greater than that estimated from particle-size distributions (Table 2), nearly an order of magnitude larger than the NRCS estimates (Table 1) and, as will be discussed later, an order of magnitude larger than the RS derived estimates of K_m; however, they are consistent with the measured values of ~900 mm/h for a fine sand surrogate for Tahoe basin soils [21].

Table 8. Summary of hydraulic conductivity measurements associated with RS plots.

	Device	RS Test Runoff?	Mean K_s (mm/h)	*CoV K_s (%)*
RS Sites—Granitic Soil				
Bliss SP	PP	Yes	896	*8.7*
Luther Pass	PP	Yes	828	*12.1*
Rubicon	PP	Yes	627	*27.5*
Bliss/Meyers—w/surfactant	MDI	No	1386	*44.5*
Angora Fire—w/ surfactant	MDI	No	1093	*42.9*
Bliss/Meyers hydrophobic	MDI	Yes	376	*118*
Heavenly LT—hydrophobic	MDI	Yes	143	*43.4*
RS Sites—Volcanic Soil				
Blackwood Cyn -Truckee –hydrophobic plots	MDI	Yes	412	*125*
Brockway Summit—2006	PP	Yes	729	*43.1*
Brockway Summit—2003	PP	Yes	558	*24.1*
Dollar Hill—Tall RS	PP	Yes	883	*9.64*
Northstar—Tall RS	PP	Yes	907	*32.3*
Homewood—Tall RS	PP	Yes	803	*27.7*
Northstar—Tall RS	PP	No	978	*23.1*
Homewood—Tall RS	PP	No	762	*22.0*
Blackwood–Truckee—w/surf.	MDI	No	871	*34.3*
Brockway—w/surfactant	MDI	No	1311	*42.4*

4. Discussion

4.1. Estimating Effective Hydraulic Conductivity K_m from RS Test Plot Data

Modeling hillslope infiltration and runoff rates requires measurement or estimation of the field effective hydraulic conductivity, K_m, some measure of the antecedent soil moisture and moisture retention conditions of the hillslope soils. Data collected from RS plot studies uniquely provides this information from a field-based assessment, though the data collected is used to infer both water retention and hydraulic conductivity parameters. Typically, the K_m value is estimated directly from the difference between the measured steady rain and runoff rates, while the infiltrated depth, V, is related to the visual wetting depth at the end of the RS test to estimate the soil water storage capacity. Alternatively, in WEPP modeling efforts, the K_m value is determined from that value which by trial and error yields the visual best-fit between the modeled runoff hydrograph assuming a single hillslope flow element and that measured during the RS test. Such a modeling fit to estimate K_m that relies on the Green–Ampt formulation of the wetting process, as outlined above in Equations (1)–(4), implicitly uses the infiltrated depth values from the RS test, but not the time-to-ponding/runoff directly, as described in Equation (8). Here, we use the individual RS plot data summarized in Tables 4 and 6 to simultaneously solve both Equations (7) and (8) using the K_m approximation for h_d from Figure 1 for sandy soils to determine the K_m value that meets both the infiltrated depth and time-to-ponding, t_p, requirements. We use time to runoff from the RS test as a conservative estimate of t_p. For the data summarized in Tables 5 and 7 for the plots not generating runoff, hence no t_p values, we use the $\Delta\theta$

value estimated from the visual wetting depth measurements and Equation (7), assuming a wetting $h_d = 50$ mm to determine K_m.

Tables 9 and 10 summarize the steady rain–runoff and infiltration-equation based K_m values from the RS runoff plots on granitic and volcanic soils, respectively, while Table 11 summarizes those K_m values for the non-runoff RS plots on both soils. Mean K_m values determined from the steady rain–runoff and infiltration equation calculations were tested for significant difference based on a two-tailed test at $p < 0.01$ and $p < 0.05$, as indicated in the tables. Mean K_m value ranges were similar for both soils (10–100 mm/h in the volcanic soils and 20–120 mm/hr in granitic soils), and overall average values were several times greater than the NRCS estimates in Table 1, though 3–4 times less than the particle-size estimated K values (Table 2) and roughly an order of magnitude less than the average permeameter and MDI estimates of K (Table 8). Overall, data collected from 20% to 25% of the RS plots resulted in undeterminable K_m values in the simultaneous solution of Equations (7) and (8). As the simultaneous infiltration equation solution is highly sensitive to the time-to-ponding/runoff value, this result suggests that those times estimated during about $\frac{1}{4}$ of the RS tests may be problematic.

Table 9. Summary of steady Rain–Runoff and Infiltration Eq. K_m values for granitic RS plots having runoff.

Non-hydrophobic Plots	Rain—Runoff K_m (mm/h)	*CoV K_m* (%)	Infilt-Eq. K_m (mm/hr)	*CoV K_m* (%)	# of UD [a] K_m
Bliss SP RC—bare	47.1 [c]	7.21	40.2	*85.1*	0
Bliss SP RC—treated	55.4	8.70	54.6	*NA* [b]	2
CalTrans BS Plots	89.9	*21.5*	UD	*NA*	3
Cave Rock/Incline Village RC	49.9	*17.0*	56.4	*30.9*	0
Heavenly CAN LT—2005	83.7 [d]	*27.2*	101	*36.7*	0
Heavenly CAN LT—2006	95.9	*NA*	UD	*NA*	1
Heavenly CAN LT—2007	96.9	*23.8*	97.6	*NA*	5
Heavenly GB MSR & OLB	97.0	*21.9*	99.2	*62.7*	7
Heavenly LRR	110	*5.0*	108	*55.1*	1
Heavenly LT—2006	79.9	*10.8*	97.0	*9.2*	0
Heavenly PON/MCD	60.4	*45.7*	57.2	*44.8*	0
Heavenly STC	99.3	*9.5*	104	*33.3*	0
Luther Pass RC	43.2	*16.7*	43.5	*19.2*	0
Mammoth	108	*9.7*	108	*44.1*	1
Meyers RC	81.8	*18.1*	82.9	*33.7*	0
Roundhill landing-	26.5	*39.0*	19.1	*83.2*	1
Roundhill landing—USFS	20.2	*47.2*	27.2	*NA*	3
Rubicon RC, treated & native	48.4	*17.7*	52.8	*10.1*	1
Truckee Bypass	72.5	*16.8*	48.5	*NA*	4
Upper Cutthroat 1D & 2T	67.3	*42.1*	90.6	*24.8*	3
Upper Cutthroat 3T	107	*7.6*	85.2	*12.7*	0
Upper Cutthroat 4T & 6T	106	*22.7*	110	*51.4*	2
Upper Cutthroat 7T	81.7	*7.6*	87.3	*24.9*	0
Upper Cutthroat 8T	98.7	*22.5*	110	*25.6*	2
Angora Fire	62.5	*30.6*	35.3	*82.6*	3
Hydrophobic plots					
Bliss SP & Meyers RC	91.0	18.72	107	24.6	0
Heavenly LT'06—Natives	37.0	*38.7*	17.7	*95.5*	0
Upper Cut. 10T & 11T	119	*1.1*	149	*1.2*	1
Upper Cut. 3N—Natives	54.0	*13.1*	41.4	*55.4*	0

[a]: UD = UnDefined values; no real solution for K_m; [b]: NA = Not Applicable usually because $n < 3$; [c]: Mean values highlighted in *RED* do not differ significantly ($p < 0.01$); [d]: Mean values highlighted in *BLUE* do not differ significantly ($p < 0.05$).

Table 10. Summary of the steady Rain–Runoff and Infiltration Equation based K_m values associated with volcanic RS plots having runoff.

Site Descriptions	Rain–Runoff K_m (mm/h)	CoV K_m (%)	Infilt. Equation K_m (mm/h)	CoV K_m (%)	# of UD [a] K_m
Blackwood Cyn–Truckee	106 [c]	12.6	117	24.9	2
Brockway Summit—2006	59.3	NA [b]	62.0	NA	0
Brockway Summit—2003	36.2	25.3	37.4	42.8	0
Dollar Hill—Tall RS	45.0	2.2	39.6	47.5	0
Homewood #31 Rd	61.8	1.7	62.1	53.0	0
Homewood LL A&B Rd	102	8.9	101	42.8	0
Homewood MAR Rd	86.5	10.6	104	25.4	2
Homewood SCD RD&BK Rd	85.7	15.9	72.9 [d]	67.5	5
Homewood WDG Rd	85.4	17.2	88.1	16.1	4
Northstar—Short RS	48.5	NA	35.8	NA	0
Juniper Mtn Skirun	40.5	19.2	26.00	73.1	0
Juniper Mtn Skirun—WCs	103	17.0	95.7	37.1	0
Northstar—Tall RS	52.5	44.8	42.2	75.8	0
Northstar—Bare ski Tall RS	37.7	16.9	28.1	48.3	5
Homewood—Tall RS	41.0	24.6	25.7	48.3	11
Northstar BP CON plots	97.6	NA	87.0	NA	1
Northstar LT	87.3	26.9	99.5	51.4	3
Northstar STA plots	102	6.8	99.0	27.5	0
Northstar Unit 7	102	NA	77.0	NA	0
Ward Cr. Landing	43.4	27.2	47.1	46.4	0
Ward Cr. Landing—USFS	23.1	13.7	9.2	NA	1

[a]: UD = UnDefined values; no real solution for K_m; [b]: NA = Not Applicable usually because $n < 3$; [c]: Mean values highlighted in *RED* do not differ significantly ($p < 0.01$); [d]: Mean values highlighted in *BLUE* do not differ significantly ($p < 0.05$).

Table 11. Summary of Infiltration Equation K_m values associated with RS plots not having runoff.

	Infilt. Equation K_m (mm/h)	CoV K_m (%)
Granite Soil Sites—Non-Hydrophobic Plots		
CalTrans OP Plots	79.7	38.6
Cave Rock—Inc. Village RCs	36.3	NA [a]
Heavenly CAN LT	42.4	29.9
Heavenly CAN LT	63.6	32.6
Heavenly GB MSR & OLB	97.3	NA
Heavenly STC	89.6	NA
Mammoth	96.7	NA
Meyers RC	58.4	23.0
Roundhill landing- IERS	35.7	NA
Truckee Bypass	84.9	18.1
Upper Cutthroat 3T	51.9	0.1
Upper Cutthroat 4T & 6T	86.2	NA
Upper Cutthroat 8T	91.7 [b]	10.5
Granite Soil Sites—Hydrophobic plots		
Bliss SP & Meyers RC—surf	115	NA
Angora Fire	50.8	NA
Upper Cut. 10T & 11T	83.3	7.0
Volcanic Soil Sites		
Blackwood–Truckee (Surf)	101	NA
Brockway Summit plots	97.5	NA
Northstar—Short RS	40.5	13.6
Northstar—Tall RS	37.2	12.0
Homewood—Tall RS	50.7	NA
Juniper Mtn Skirun	42.9	50.4
Northstar BTD & BP CON	97.5	NA
Northstar LT	55.2	41.3
Northstar Unit 7—Short RS	75.2	24.9

[a]: NA = Not Applicable usually because $n < 3$; [b]: Mean values highlighted in *RED* between sister runoff plots do not differ significantly ($p < 0.01$).

For roughly 80% of the RS sites on both soils, the simpler rain–runoff rate estimate of K_m values was essentially equivalent to that obtained from the infiltration equation solution, lending credence to use of the rain–runoff rate estimates of K_m for watershed modeling purposes. Considering K_m values estimated from Equation (7) for the RS plots lacking runoff, there was some agreement between the rain–runoff rate K_m values from the sister plots as indicated in Table 11, but few direct comparisons were available. On the other hand, the overall soil average rain–runoff rate K_m values of 73.2 and 68.9 mm/h from the granitic and volcanic runoff RS plots, respectively, were essentially equivalent to the Equation (7) estimates from the non-runoff RS plots of 72.7 and 66.4 mm/h, respectively. Thus, use of the Equation (7), combined with visual estimation of the $\Delta\theta$ values (e.g., Figure 2), appears to also be a reasonable estimate of K_m values for modeling purposes. Finally, to illustrate some of the variability in the comparison between both estimates of K_m values as well as determining any possible bias, Figures 4 and 5 show comparisons of the K_m values summarized in Tables 9 and 10, respectively. Interestingly, for the granitic soils, infiltration equation K_m values appear to be a slightly greater on average (~3%) as compared to the rain–runoff rate estimates for the granitic soils, while for the volcanic soils, they are on average ~4% less, such that, overall across all RS plots, there appears to be no systematic bias or preference between the two methods of estimating K_m values.
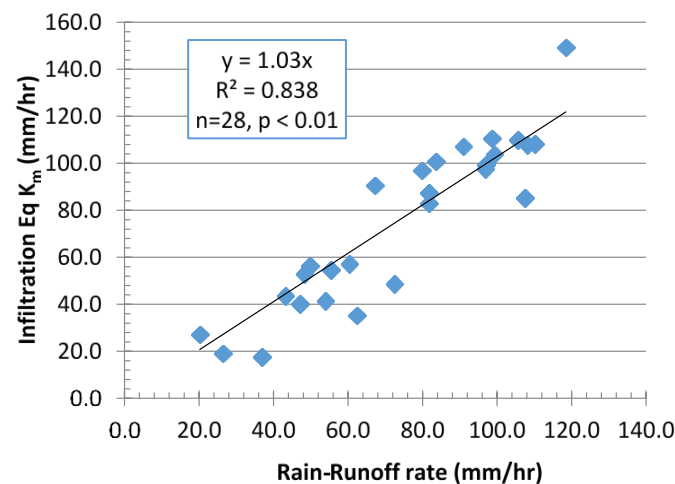

Figure 4. Dependence of Infiltration Equation K_m values on Rain–Runoff rates for granitic soil RS plots having runoff.
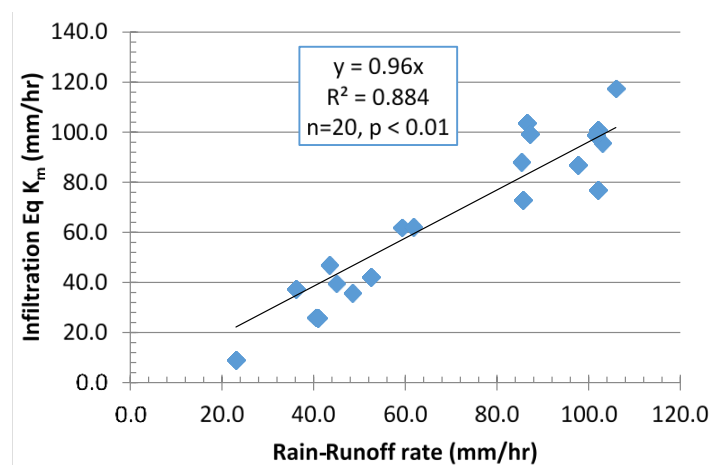

Figure 5. Dependence of Infiltration Equation K_m values on Rain–Runoff rates for volcanic soil RS plots having runoff.

4.2. Runoff Erosion Field Data—How Are Sediment Detachment Rates Related to Stream Power?

Perhaps one of the primary purposes of RS plot studies is to estimate surface runoff transport rates of sediment and other contaminants so as to develop the required watershed parameters, or evaluate the relative success of soil restoration efforts. Using sediment detachment rates measured from the short DF RS plots on granitic roadcuts on the south west shore and volcanic soil skiruns of the north shore of Lake Tahoe, we evaluate whether turbulent or laminar flow stream power (Equations (19) or (20)) are appropriate to describe these rates. As summarized in Tables 4 and 6, these RS test plots were on a broad range of slopes and used rainfall rates from 60 to 120 mm/h, with test durations of 30–60 min. While occasionally there was no runoff from the treated or grassed RS plots, these data were not included in the comparisons; however, multiple non-runoff plots in the restored and native soils were represented by two zero values in the analyses. The soil surface conditions included no cover (bare) to light grasses, treated soils (usually pine-needle or woodchip mulch covers), restored soils (incorporated mulches and tillage) and "native" (relatively undisturbed forest soils adjacent to RS test sites). We graph average RS plot soil detachment rates ($\times 10^5$ kg/m^2/s) per condition (usually *n* = 3) as a function of $q^{0.67}S^{1.328}$ from Equation (20) to estimate the effective "erodibility" as it depends on stream power in Figure 6 for the granitic soils, and in Figures 7 and 8 for the volcanic soils. Note that the soil detachment rates from the finer-textured volcanic soils are much greater than those from the granitic soils in general. Similarly, considering the linear slopes of the regressions to represent soil "erodibility", erodibilities from the bare granitic and grassed volcanic soils were roughly equivalent, while those from restored and native (undisturbed) volcanic soils were effectively identical, though about three times greater than equivalently treated or native granitic soils. Lastly, comparing sediment detachment rates as a function of the product of the rainfall rate and stream power dramatically lowered the R^2 values in all of the regressions, suggesting that at least for the rainfall rates/energies, infiltration rates and soil cover conditions considered here, rainfall rates had little impact on soil erodibility.
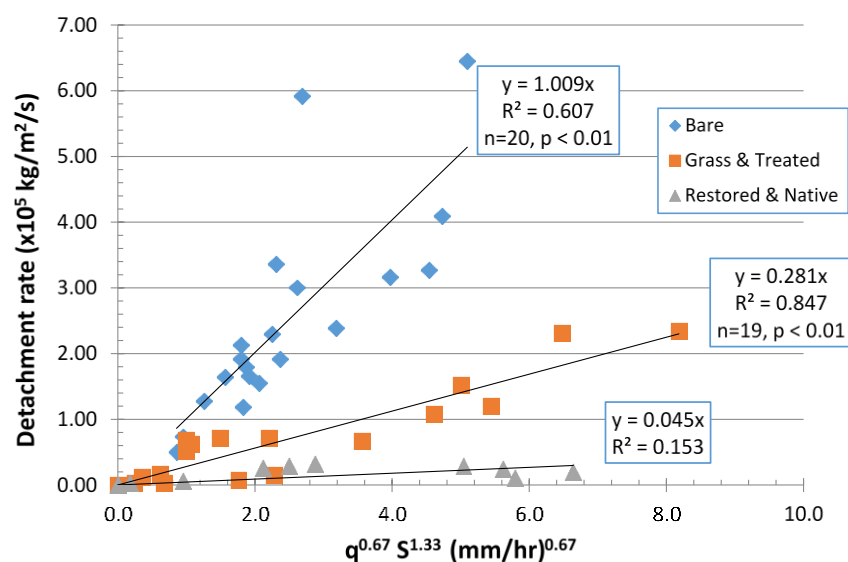

Figure 6. Comparison between and stream power variables for granitic RS plots on the southwest shore of Lake Tahoe.
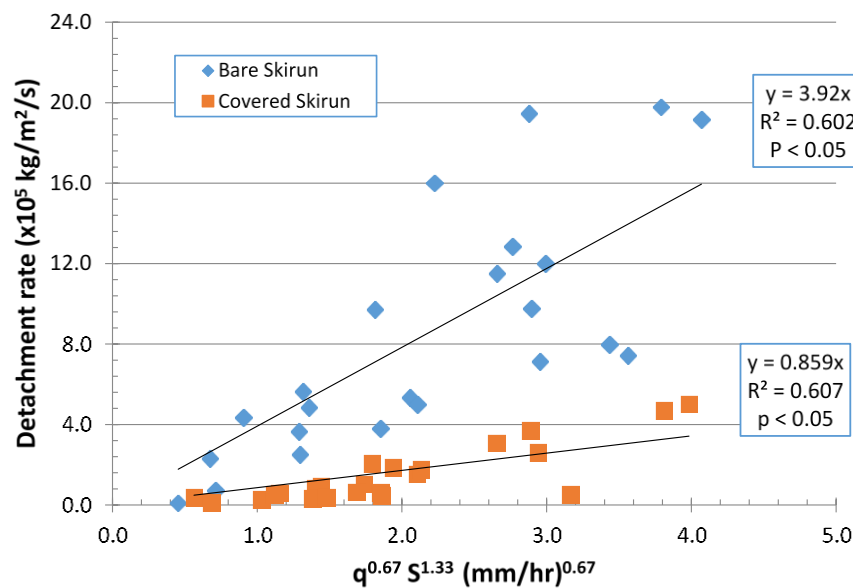
Figure 7. Comparison between and stream power variables for bare and grass-covered volcanic RS plots on the northwest shore of Lake Tahoe.
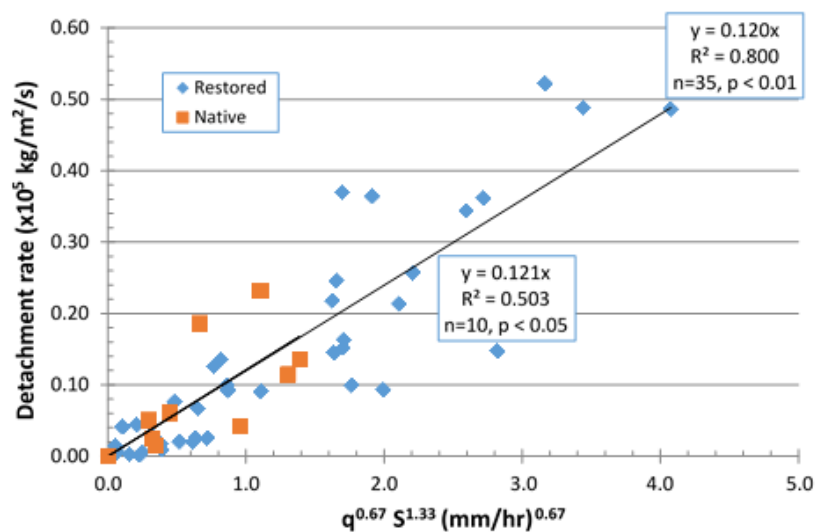

Figure 8. Comparison between and stream power variables for bare and grass-covered volcanic RS plots on the northwest shore of Lake Tahoe.

As a means of assessing the hypothesis that laminar flow definition of stream power by Equation (20) better describes the sediment detachment rates than that from turbulent flow assumptions using Equation (19), we examined the regression coefficient variation as it depends on the exponent of the surface runoff rate for the data shown in Figures 6–8. It should be noted, of course, that soil detachment rates as determined from the RS plot runoff sediment concentrations result in a degree of self-correlation with runoff rates as both are calculated from the runoff sampling data. Considering the regression coefficient variation provides some insight into the range of stream power exponent values reported in the literature and perhaps why they range from theoretical values. Figure 9 illustrates the dependence of the linear regression R^2 value on the exponent of q in Equation (20) for the granitic soils of Figure 6, while Figure 10 illustrates this same dependence for the volcanic RS test plot data shown in

Figures 7 and 8. For the granitic RS test plots, the greatest R^2 value occurs as predicted by Equation (20) at $q^{0.67}$ for the grassed and treated RS plots, and this is also near the maximum R^2 value for the bare plots. In both cases, however, the R^2 values at $q^{0.67}$ readily exceed those for $q^{0.4}$ from Equation (19), but the relative dependence of the R^2 value is "flat" for exponents ranging from 0.8 to 1.3, as found by Al-Hamdan et al. [35]. The sediment detachment rates from the restored and native granitic RS test plots are so small and variable as to have little discernible dependence on stream power. In the volcanic RS test plots, the greatest R^2 value again occurs as predicted by Equation (20) at $q^{0.67}$ for the grassed and treated RS plots, and this is also near the maximum R^2 value for the bare plots. As with the bare granitic RS plot data, the R^2 value for the volcanic RS plots has little dependence on the runoff rate exponent at values greater than about 0.8, but these R^2 values differ little from that associated with an exponent of 0.67. For the bare and native volcanic RS test plots, the greatest R^2 values occur at an exponent of 1.1. In all volcanic RS plots, however, the R^2 values at $q^{0.67}$ readily exceed those for $q^{0.4}$ from Equation (19), suggesting that, as with the granitic soils, the soil detachment rate is better described by laminar as compared to turbulent flows for the Tahoe soils.
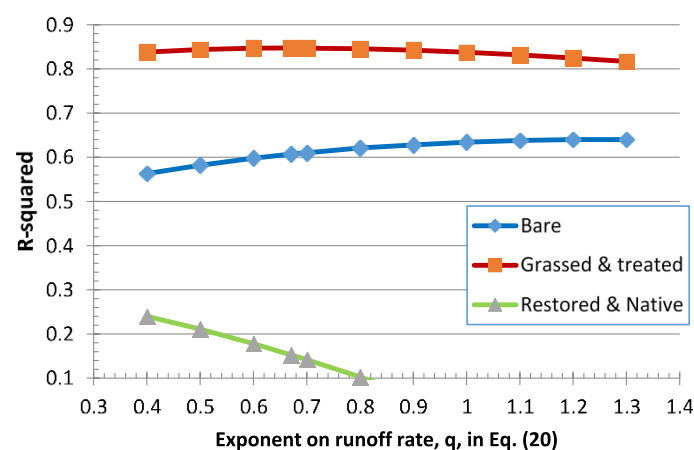

Figure 9. Dependence of linear regression R^2 values on exponent of runoff rate in stream power function when related to soil detachment rates from granitic RS plots.
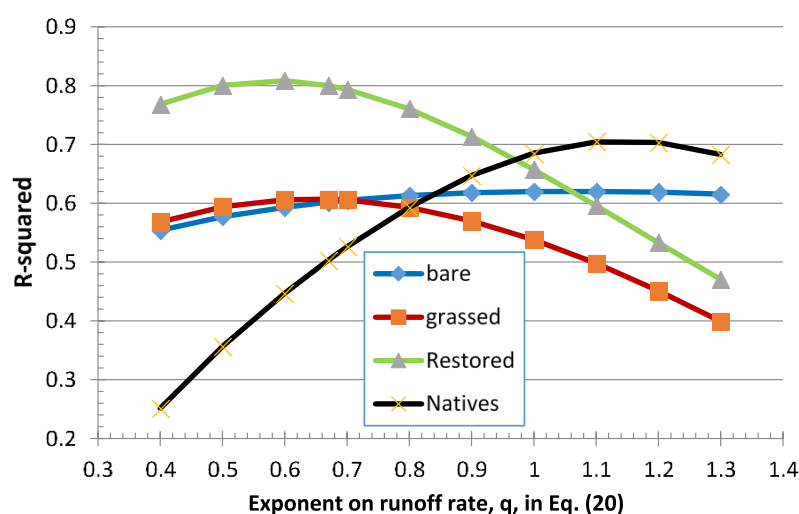

Figure 10. Dependence of linear regression R^2 values on exponent of runoff rate in stream power function when related to soil detachment rates from volcanic RS plots.

Finally, defining RS plot erodibility as the linear regression slope between soil detachment rates, D_i, and laminar stream power, P, or average ratio thereof, the erodibilities likely useful for watershed modeling in the Tahoe basin are summarized in Table 12 from the results shown in Figures 6–8. Of course, as the values in Table 12 were derived from the runoff plots from the restored and less-disturbed forest (native) soil conditions, they are likely conservative estimates as there were numerous non-runoff RS plots for these conditions.

Table 12. Summary of stream power (Equation (20)) derived soil erodibility for granitic and volcanic soil RS plots from the southwest and north shores of Lake Tahoe, respectively.

Soil Type	Erodibilities for Soil Condition = D_i/P (s^2/m)			
	Bare	**Grass Cover**	**Treated**	**Restored/Native**
Granitic	3.35×10^{-5}	0.93×10^{-5}		0.15×10^{-5}
Volcanic	16.0×10^{-5}	2.20×10^{-5}		0.40×10^{-5}

4.3. Results & Discussion of Rainfall Simulator Comparisons—Infiltration & Erosion Processes

With the several types of "portable" RS devices used in field plot studies that have a variety of rainfall energies applied to plot areas in the order of one square meter, comparing plot test results (infiltration, runoff and erosion rates) from these different RSs has been a recurring challenge in the literature. Having outlined above possible interpretations methods for determination of infiltration (K_m) and erosion parameter averages from the entire range of RS test plots across the Tahoe Basin, here, we consider the more specific site evaluation of RS test plots using different RSs to determine how simulators with different rain energies may affect these parameters. We focus on a direct comparison of the infiltration and erosion results obtained from three RSs used in the basin that have rain drop energies of $<\frac{1}{4}$ and about $\frac{3}{4}$ of maximum values (i.e., short and tall drop-former (DF) simulators, respectively) and the greater energy sprinkler RS used by the USFS. We use RS plot data for the short and tall DF RSs at similar Northstar disturbed and treated volcanic soil sites, and likewise, we use plot data for the short DF and USFS RSs at soil forest landings on the west and east shores of the lake. First, we compare soil K_m values estimated from steady rain–runoff rates and simultaneous solutions to the infiltration equations, as described above, then we consider the estimated erodibilities (D_i/P) from the different RSs, as in Table 12 for the same sites.

In the Northstar area, there were several skirun, or adjacent sites, that included RS tests with both the original tall DF RS and the short DF RS on bare and treated soils from different years. The average plot information for the Northstar sites is in Table 6 for the runoff plots, while the plot-specific erosion information is summarized in Table 13. Overall, the average plot slopes for both DF RS plots were similar, however, the short DF RS plots were subject to rain rates twice as great (120 *vs.* 60 mm/h) as that for the tall DF RS plots, though with about 30% less impact energy. The average of the 14 K_m values estimated from the bare and treated soil plot data for the tall DF RS was, surprisingly, roughly half that for the 11 short DF RS test plots subjected to the much greater rain rate. However, the comparison between infiltration equation and rain–runoff rate estimates are functionally the same, as shown in Figure 11.
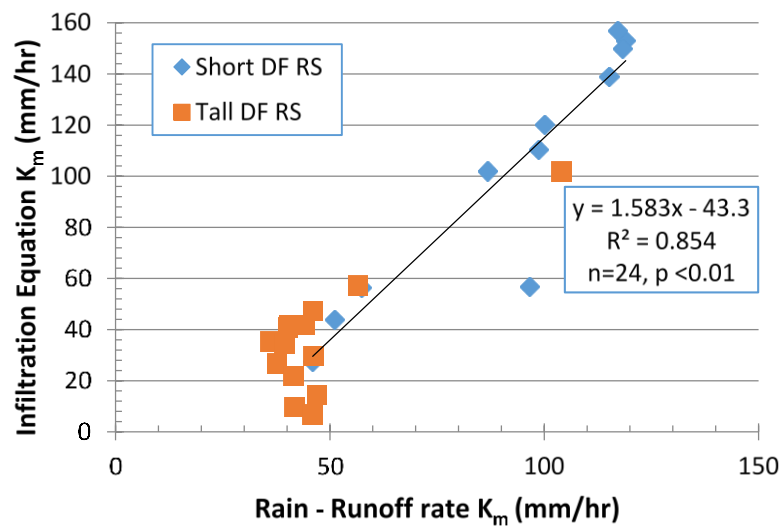
Figure 11. Dependence of Infiltration-equation K_m values on Rainfall–Runoff rates for the short and tall DF type RS at Northstar ski area (volcanic soils).

Table 13. Summary of plot data for stream power derived soil erodibility for volcanic bare and treated soil RS plots using the tall and short DF type RSs at Northstar ski area.

Soil Condition (Short or Tall DF RS)	Slope (%)	Steady q (mm/h)	SY [a] (gm/mm)	$D_i \times 10^5$ (kg/m^2/s)	D_i/P (s^2/m)
	60.7	19.6	23.2	19.8	1.73×10^{-4}
	42.1	26.9	16.6	19.5	2.24×10^{-4}
Bare soils (Tall DF)	37.0	23.6	15.6	16.0	2.39×10^{-4}
	31.7	23.7	9.4	9.71	1.78×10^{-4}
	25.6	22.4	5.8	5.64	1.42×10^{-4}
Averages	39.4	23.3	14.1	14.1	19×10^{-5}
	27.6	10.9	0.35	0.16	6.07×10^{-6}
	27.3	16.2	0.20	0.14	4.04×10^{-6}
Treated [b] soils (Tall DF)	35.0	10.9	0.60	0.28	7.64×10^{-6}
	35.0	5.7	0.30	0.08	3.12×10^{-6}
	36.4	16.7	0.40	0.29	5.55×10^{-6}
Averages	32.3	12.1	0.37	0.19	0.53×10^{-5}
Light grass soil covers (Short DF)	47.7	24.4	3.62	3.82	3.99×10^{-5}
	51.0	15.9	6.25	4.33	5.48×10^{-5}
	47.9	20.1	2.89	2.52	2.97×10^{-5}
Averages	48.9	20.1	4.25	3.56	4.15×10^{-5}
	34.5	24.6	0.16	0.17	2.72×10^{-6}
	31.1	5.3	0.16	0.04	1.88×10^{-6}
	32.9	19.1	0.26	0.22	4.38×10^{-6}
Treated soils (Short DF)	31.9	22.6	0.15	0.15	2.84×10^{-6}
	35.5	6.3	0.14	0.04	1.44×10^{-6}
	35.9	12.6	0.16	0.09	2.09×10^{-6}
	33.9	10.0	0.26	0.11	3.42×10^{-6}
Averages	33.7	14.4	0.19	0.12	0.27×10^{-5}

[a]: SY = Sediment yield expressed as mass of sediment per mm of runoff determined from slope of accumulated sediment *versus* accumulated runoff from the RS plot (Grismer & Hogan, 2004); [b]: Various combinations of tilled compost, pine needle mulch and wood chips plot covers.

Despite the much greater rain impact energies and greater runoff rates from the tall *versus* short DF RSs, erodibilities expressed as D_i/P were only slightly greater for the tall RS plots, though practically the same for these bare volcanic skirun soils (19×10^{-5} *vs.* 16×10^{-5} s^2/m). Similarly, for the lightly

covered plots, the short DF RS plots at the Northstar specific site were greater than at the skirun average (~4×10^{-5} *vs.* ~2×10^{-5} s^2/m), perhaps due to varying coverages. While mean erodibility values from the tall DF RS for the "treated" plots were twice as great as those from the short DF RS plots (0.53×10^{-5} *vs.* 0.27×10^{-5} s^2/m), these values ranged on either side of that mean in Table 12 (0.4×10^{-5} s^2/m) for the short DF RS plots. Moreover, the difference between the means was similar to the variability in values between individual RS plots from either RS, and may have reflected the different years of RS tests or variability in treatments. We note that the average runoff organic matter fraction (OM%) from the treated RS plots was ~25%, suggesting presence of some non-mineral soil cover.

In a more direct comparison of results from different RSs, the short DF RS and the USFS sprinkler RS were used on compacted soil forest landing sites near Ward Creek (volcanic soil) and at Round Hill (granitic soil) using randomly selected plots from within the same area and conducting the RS tests on the same days. The average plot information for these sites is in Tables 4 and 6 for the runoff plots while the plot-specific erosion information is summarized in Table 14. Overall, the RS plot slopes for the DF RS were about half that for the USFS RS, and the DF RS rain rates were also 10–20 mm/h less, as well as having much smaller rain impact energies as compared to the sprinkler RS. As a result, times-to-runoff and runoff rates from the DF RS plots were smaller than those from the sprinkler RS. Finally, one USFS plot at Round Hill responded completely differently than its sister plots and was not included in the erosion analysis.

Table 14. Summary of plot data for stream power derived soil erodibility for granitic and volcanic soil forest landing RS plots for short DF RS and USFS sprinkler RS.

Site (DF or USFS RS)	Soil Condition	Slope (%)	Steady q (mm/h)	SY [a] (gm/mm)	$D_i \times 10^5$ (kg/m^2/s)	D_i/P (s^2/m)
Round Hill (DF)	Bare	3.4	51.1	0.41	0.91	19.3×10^{-5}
	Light PN mulch cover	6.5	23.8	0.98	1.01	15.1×10^{-5}
	PN mulch cover, grass	10.4	38.1	0.20	0.33	1.93×10^{-5}
	PN Mulch & WC cover	4.7	54.5	0.06	0.14	1.87×10^{-5}
	Tilled PNM [b] & WC cover	6.1	45.2	0.02	0.04	0.42×10^{-5}
Round Hill (USFS)	Bare	17.1	69.3	4.53	8.72	20.5×10^{-5}
	Light PN mulch cover	14.2	69.6	2.93	5.66	17.0×10^{-5}
	Light PN mulch cover	22.1	71.9	3.51	7.01	11.4×10^{-5}
Ward Cr. (DF)	Bare ~5% mulch cover	6.7	41.2	1.93	3.45	34.3×10^{-5}
	PN Mulch & WC cover	7.0	19.5	0.17	0.14	2.23×10^{-5}
	PN Mulch & WC cover	7.0	14.9	0.19	0.12	2.28×10^{-5}
	PN Mulch & WC cover	8.7	30.7	0.18	0.24	2.05×10^{-5}
Ward Cr. (USFS)	Bare ~5% mulch cover	10.3	62.3	2.86	4.949	24.4×10^{-5}
	Light PN mulch cover	21.2	71.0	2.37	4.674	8.11×10^{-5}
	Light PN mulch cover	22.8	71.6	1.67	3.321	5.20×10^{-5}

[a]: SY = Sediment yield expressed as mass of sediment per mm of runoff determined from slope of accumulated sediment *versus* accumulated runoff from RS plot [46]; [b]: PNM = Pine needle mulch, WC = wood chips plot covers.

When considering K_m estimates developed from all RS plot data collected from the two forest landing sites, we found that of the seven USFS RS plots, only three yielded data that enabled computation of K_m from the combined infiltration equations, while eight of the nine short DF RS plots yielded calculable K_m values. At the Round Hill site, the average K_m values from both calculation methods were the same, at about 23 mm/hr. At the volcanic soil Ward Creek site, the DF RS plot average K_m values were more than twice that obtained from the neighboring USFS RS plots. Following the same format as in Figures 4 and 5, the forest landings K_m values are graphed in Figure 12. Both types of RSs resulted in infiltration equation *versus* rain–runoff rate estimated K_m values fitting the same line as well as being consistent with the WEPP based K_m values. Similarly, despite the differing rain impact energies from the two RSs, erodibilities expressed as D_i/P were practically the same for the bare granitic soils (~20×10^{-5} s^2/m) and the lightly covered plots (~15×10^{-5} s^2/m). Erodibility values for

the better covered RS plots were approximately 1.9×10^{-5} s^2/m, consistent with the "grass/treated soils" value in Table 12. On the volcanic soils, the bare plot erodibilities differed between the two RSs (~24×10^{-5} *vs.* 34×10^{-5} s^2/m), but well within the variability range encountered in replicate plots results. These erodibility values were roughly two times greater than that from the bare skiruns in Table 12, likely reflecting the greater soil compaction at the forest landings. The one tilled-in mulch plot yielded an erodibility value equal to that average found for the "treated/restored" volcanic skirun soils (Table 12). This treated soil plot suggests the possibility that even the compacted forest landing soils may be "treatable" to the point of returning them to something like native forest soil functionality with respect to infiltration and erosion. Finally, we note that the OM% of the runoff from the DF RS plots were quite high (30%–50%), suggesting that visual assessment of the surface conditions as "bare" or "light coverage" likely overlooked the possibility of an apparent fine mulch/duff organic layer integrated with the mineral soil surface.
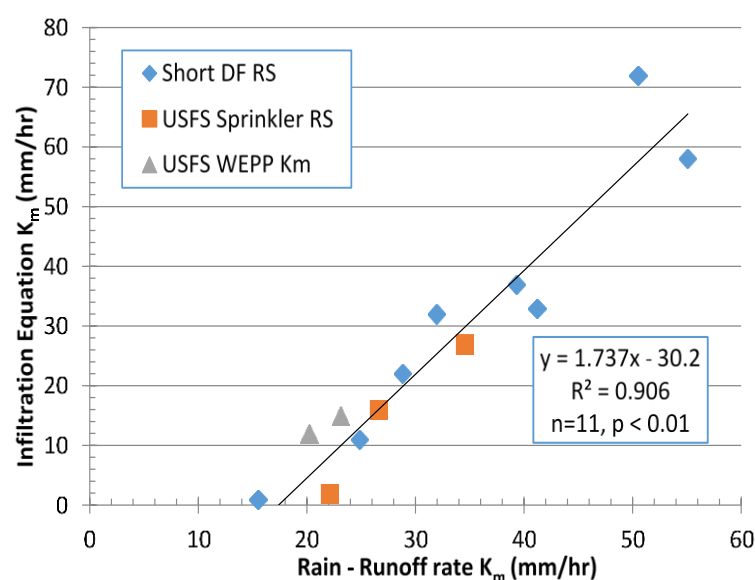

Figure 12. Dependence of Infiltration equation K_m values on Rainfall-Runoff rates for the short DF and Sprinkler type RSs from tests plots at Ward Creek and Round Hill forest landings.

5. Summary & Conclusions

A key component of modeling watershed runoff and erosion processes is estimation of surface soil infiltration rates or effective hydraulic conductivities (K_m) and erosion rates, as they vary with soil cover/tilth/slope conditions, and seasonally with changing water contents. Portable rainfall simulators (RSs) are essential tools for measuring infiltration, runoff and erosion under a variety of field conditions, and information from RS test plots can provide the infiltration/runoff parameterization required for watershed modeling. Though multiple RS designs for field application exist, no single RS design (including plot runoff frame installation) has emerged as a standard. Here, we develop a simultaneous solution of time-to-ponding/runoff and Green–Ampt type infiltration equations to determine K_m, as well as developing a laminar flow-based description of stream power that can be used to determine erodibilities and then apply these analyses to data from 423 RS plots across the Tahoe Basin. Finally, we provide direct infiltration and erosion analysis comparisons of results from three RSs that have different rainfall energies. The overall goal of the analyses was to develop a common assessment method, or approach, to evaluating RS plot data for use in watershed modeling efforts.

With respect to estimation of K_m values, the simpler-to-calculate steady rain–runoff rate value was equivalent for all practical purposes to that estimated from infiltration equations. It was possible to calculate infiltration equation based K_m values from ~80% of the RS plot data that spanned a

wide range of rain rates (60–120 mm/h), runoff rates (2–70 mm/h) and times-to-ponding (1–20 min). However, this effective conductivity, though assumed to be half of the saturated value, was as much as an order of magnitude less than K_s values derived from other field test methods. In terms of developing comparable "erodibilities", defined here as simply the ratio of sediment detachment rates to stream power, it appears that the laminar flow derived stream power results in a better fit between detachment rate and stream power than that derived from turbulent flow assumptions, and eliminates the need to define 'n' and the restriction to <10% slopes associated with the Mannings equation. Applying the laminar flow stream power derivation to the determination of erodibilities enabled comparison of data from RS test plots having a wide range of slopes and runoff rates, as well as from simulators having different rainfall energies. While rain drop impact energy did not appear to be a factor in these analyses, this may stem from the presence of some cover materials, the very high infiltration rates and the lack of aggregation of the Tahoe surface soils. We suggest, as Grismer [50] did, that RS plot studies include measurements of particle sizes and OM% in the runoff collected in order to provide more useful data from which to understand erosional processes and soil restoration efforts.

Conflicts of Interest: The authors declare no conflict of interest.

References

1. Amerman, C.R. Rainfall simulation as a research tool in infiltration. In Proceedings of the Rainfall Simulator Workshop, Tuscon, AZ, USA, 7–9 March 1979.
2. Grismer, M.E. Standards vary in studies using rainfall simulators to evaluate erosion. *Calif. Agric.* **2012**, *66*, 102–107. [CrossRef]
3. Grismer, M.E. Rainfall Simulation Studies—A Review of Designs, Performance and Erosion Measurement Variability. Review for the Tahoe Science Consortium. 2011, 110. Available online: http://ucanr.org/sites/californiaagriculture/files/145682.pdf (accessed on 1 June 2016).
4. Iserloh, T.; Ries, J.B.; Arnáez, J.; Boix-Fayos, C.; Butzen, V.; Cerdà, A.; Echeverría, M.T.; Fernández-Gálvez, J.; Fister, W.; Geißler, C.; et al. European small portable rainfall simulators: A comparison of rainfall characteristics. *Catena* **2013**, *110*, 100–112. [CrossRef]
5. Gallart, F.; Llorens, P.; Latron, J.; Regüés, D. Hydrological processes and their seasonal controls in a small Mediterranean mountain catchment in the Pyrenees. *Hydrol. Earth Syst. Sci.* **2002**, *6*, 527–537. [CrossRef]
6. Hessel, R. Modelling soil erosion in a small catchment on the Chinese Loess Plateau: applying LISEM to extreme conditions. *Neth. Geogr. Stud.* **2002**, *307*, 1–21.
7. García-Ruiz, J.M.; Lana-Renault, N.; Beguería, S.; Lasanta, T.; Regüés, D.; Nadal-Romero, E.; Serrano-Muela, P.; López-Moreno, J.I.; Alvera, B.; Martí-Bono, C.; et al. From plot to regional scales: Interactions of slope and catchment hydrological and geomorphic processes in the Spanish Pyrenees. *Geomorphology* **2010**, *120*, 248–257. [CrossRef]
8. Pan, C.; Shangguan, Z. Runoff hydraulic characteristics and sediment generation in sloped grassplots under simulated rainfall conditions. *J. Hydrol.* **2006**, *331*, 178–185. [CrossRef]
9. Pardini, G.; Gispert, M.; Dunjo, G. Relative influence of wildfire on soil properties and erosion processes in different Mediterranean environments in NE Spain. *Sci. Total Environ.* **2004**, *328*, 237–246. [CrossRef] [PubMed]
10. Seeger, M. Uncertainty of factors determining runoff and erosion processes as quantified by rainfall simulations. *Catena* **2007**, *71*, 56–67. [CrossRef]
11. Boer, M.; Puigdefábregas, J. Effects of spatially structured vegetation patterns on hillslope erosion in a semiarid Mediterranean environment: a simulation study. *Earth Surf. Process. Landf.* **2005**, *30*, 149–167. [CrossRef]
12. Nadal-Romero, E.; Lasanta, T.; Regüés, D.; Lana Renault, N.; Cerdá, A. Hydrological response and sediment production under different land cover in abandoned farmland fields in a Mediterranean mountain environment. *Bull. Assoc. Spanish Geogr.* **2011**, *55*, 303–323.
13. Stoffel, M.; Wilford, D.J. Hydrogeomorphic processes and vegetation: Disturbance, process histories, dependencies and interactions. *Earth Surf. Process. Landf.* **2012**, *37*, 9–22. [CrossRef]

14. Battany, M.C.; Grismer, M.E. Development of a portable field rainfall simulator system for use in hillside vineyard runoff and erosion studies. *Hydrol. Proc.* **2000**, *14*, 1119–1129. [CrossRef]

15. Battany, M.C.; Grismer, M.E. Rainfall runoff, infiltration and erosion in hillside vineyards: Effects of slope, cover and surface roughness. *Hydrol. Proc.* **2000**, *14*, 1289–1304. [CrossRef]

16. Lascelles, B.; Favis-Mortlock, D.T.; Parsons, A.J.; Guerra, A.J.T. Spatial and temporal variation in two rainfall simulators: Implications for spatially explicit rainfall simulation experiments. *Earth Surf. Process. Landf.* **2000**, *25*, 709–721. [CrossRef]

17. Kinnell, P.I.A. Raindrop-impact-induced erosion process and prediction: a review. *Hydrol. Proc.* **2005**, *19*, 2815–2844. [CrossRef]

18. Kinnell, P.I.A. Simulations demonstrating interaction coarse and fine sediment loads in rain-impacted flow. *Earth Surf. Process. Landf.* **2006**, *31*, 355–367. [CrossRef]

19. Grismer, M.E. Pore-size distribution and infiltration. *Soil Science* **1986**, *141*, 249–260. [CrossRef]

20. Morel-Seytoux, H.J. Application of infiltration theory for determination of excess rainfall hyetograph. Water Resources Bulletin. *Am. Water Resour. Assoc.* **1981**, *17*, 1012–1022. [CrossRef]

21. Grismer, M.E. Runoff simulations and watershed modeling. *Hydrology* **2016**, *3*, 18–30. [CrossRef]

22. Benjamin, T.B. Wave formation in laminar flow down an inclined plane. *J. Fluid Mech.* **1957**, *2*, 554–574. [CrossRef]

23. Ellison, W.D. Soil erosion studies. Part I. *Agric. Eng.* **1947**, *28*, 145–146.

24. Fristensky, A.; Grismer, M.E. A modeling approach for ultrasonic soil aggregate stability assessment. *Catena* **2008**, *74*, 153–164. [CrossRef]

25. Fristensky, A.; Grismer, M.E. Evaluation of ultrasonic aggregate stability and rainfall erosion resistance of disturbed and amended soils in the Lake Tahoe Basin, USA. *Catena* **2009**, *79*, 93–102. [CrossRef]

26. Owoputi, L.O.; Stolte, W.J. Soil detachment in the physically based soil erosion process: A review. *ASAE Trans.* **1995**, *38*, 1099–1110. [CrossRef]

27. Foster, G.R.; Meyer, L.D. Transport of soil particles by shallow flow. *ASAE Trans.* **1972**, *15*, 99–102. [CrossRef]

28. Bridge, J.S.; Dominic, D.F. Bed load grain velocities and sediment transport rates. *Water Resour. Res.* **1984**, *20*, 476–490. [CrossRef]

29. Gilley, J.E.; Finkner, S.C. Estimating soil detachment caused by raindrop impact. *ASAE Trans.* **1985**, *26*, 140–146. [CrossRef]

30. Gilley, J.E.; Woolhiser, D.A.; McWhorter, D.B. Interrill soil erosion—Part I: Development of model equations. *ASAE Trans.* **1985**, *26*, 147–153. [CrossRef]

31. Gilley, J.E.; Woolhiser, D.A.; McWhorter, D.B. Interrill soil erosion—Part II: Testing and use of model equations. *ASAE Trans.* **1985**, *26*, 154–159. [CrossRef]

32. Moore, I.D.; Burch, G.J. Sediment transport capacity of sheet and rill flow: Application of unit stream power theory. *Water Resour. Res.* **1986**, *22*, 1091–1107. [CrossRef]

33. Grismer, M.E. Soil Restoration and Erosion Control: Quantitative Assessment in Rangeland and Forested areas. *ASABE Trans. Soil Water Centen. Collect.* **2007**, *50*, 1619–1626. [CrossRef]

34. Gabriels, D.M. The Stream Power Concept in Estimating Sediment Transport. Available online: http://indico.ictp.it/event/a12165/session/37/contribution/30/material/0/0.pdf (accessed on 1 June 2016).

35. Al-Hamdan, O.Z.; Pierson, F.B.; Nearing, M.A.; Williams, C.J.; Stone, J.J.; Kormos, P.R.; Boll, J.; Weltz, M.A. Concentrated flow erodibility for physically based erosion models: Temporal variability in disturbed and undisturbed rangelands. *Water Resour. Res.* **2012**. [CrossRef]

36. Zhang, F.-B.; Wang, Z.-L.; Yang, M.-Y. Validating and Improving Interrill Erosion Equations. *PLoS ONE* **2014**. [CrossRef] [PubMed]

37. McCool, D.K.; Brown, L.C.; Foster, G.R.; Mutchler, C.K.; Meyer, L.D. Revised slope steepness factor for the universal soil loss equation. *ASAE Trans.* **1987**, *30*, 1387–1396. [CrossRef]

38. Zhang, G.H.; Liu, B.Y.; Nearing, M.; Zhang, K.L. Soil detachment by shallow flow. *ASAE Trans.* **2002**, *45*, 351–357.

39. Zhang, G.H.; Liu, B.Y.; Liu, G.B.; He, X.; Nearing, M. Detachment of undisturbed soil by shallow flow. *Soil Sci. Soc. Am. J.* **2003**, *67*, 713–719. [CrossRef]

40. Nearing, M.A.; Parker, S.C. Detachment of soil by flowing water under turbulent and laminar conditions. *Soil Sci. Soc. Am. J.* **1994**, *58*, 1612–1614. [CrossRef]

41. Guy, B.T.; Dickinson, W.T.; Rudra, R.P. The roles of rainfall and runoff in the sediment transport capacity of interrill flow. *ASAE Trans.* **1987**, *30*, 1378–1386. [CrossRef]

42. Sharma, P.P.; Gupta, S.C.; Foster, G.R. Predicting soil detachment by raindrops. *Soil Sci. Soc. Am. J.* **1993**, *57*, 674–680. [CrossRef]

43. Sharma, P.P.; Gupta, S.C.; Foster, G.R. Raindrop-induced soil detachment and sediment transport from interrill areas. *Soil Sci. Soc. Am. J.* **1995**, *59*, 727–734. [CrossRef]

44. Sharma, P.P.; Gupta, S.C.; Rawls, W.J. Soil detachment by single raindrops of varying kinetic energy. *Soil Sci. Soc. Am. J.* **1991**, *55*, 301–307. [CrossRef]

45. Lei, T.W.; Zhang, Q.W.; Zhao, J. A laboratory study on sediment transport capacity in the dynamic process of rill erosion. *Trans. ASAE* **2001**, *44*, 1537–1542.

46. Grismer, M.E.; Hogan, M.P. Evaluation of Revegetation/Mulch Erosion Control Using Simulated Rainfall in the Lake Tahoe Basin: 1. Method Assessment. *Land Degrad. Dev.* **2004**, *13*, 573–588. [CrossRef]

47. Grismer, M.E.; Hogan, M.P. Evaluation of Revegetation/Mulch Erosion Control Using Simulated Rainfall in the Lake Tahoe Basin: 2. Bare Soil Assessment. *Land Degrad. Dev.* **2005**, *16*, 397–404. [CrossRef]

48. Grismer, M.E.; Hogan, M.P. Evaluation of Revegetation/Mulch Erosion Control Using Simulated Rainfall in the Lake Tahoe Basin: 3. Treatment Assessment. *Land Degrad. Dev.* **2005**, *16*, 489–501. [CrossRef]

49. Grismer, M.E.; Ellis, A.L.; Fristensky, A. Runoff Sediment Particle-sizes associated with Soil Erosion in the Lake Tahoe Basin, USA. *Land Degrad. Dev.* **2008**, *19*, 331–350. [CrossRef]

50. Grismer, M.E.; Shnurrenberger, C.; Arst, R.; Hogan, M.P. Integrated Monitoring and Assessment of Soil Restoration Treatments in the Lake Tahoe Basin. *Environ. Monit. Assess.* **2009**, *150*, 365–383. [CrossRef] [PubMed]

51. Rice, E.C.; Grismer, M.E. Dry-season soil-water repellency effects on infiltration rates in the Tahoe Basin. *Calif. Agric.* **2010**, *64*, 141–148. [CrossRef]

52. Foltz, R.B.; Luce, C.H.; Stockton, P. The Kinetic Energy Field Under a Rainfall Simulator. In *Watershed Management Planning for the 21st Century*; Committee on the Water Resources Engineering Division/ASCE: San Antonio, TX, USA; 1995.

53. NRCS, Soil Survey Staff, USDA. Soil Survey of the Tahoe Basin Area, California and Nevada, 2007. Available online: www.websoilsurvey.nrcs.usda.gov (accessed on 7 June 2016).

54. Robichaud, P.R.; Lewis, S.A.; Ashmun, L.E. *New Procedure for Sampling Infiltration to Assess Post-Fire Soil Water Repellency*; U.S. Department of Agriculture, Forest Service, Rocky Mountain Research Station: ReFort Collins, CO, USA; 2008; p. 14.

55. Johnson, L.K. Precision Permeameter Manual; Measuring saturated hydraulic conductivity of earthen materials in the vadose zone. Unpublished material, 2001.

56. Zangar, C.N. *Theory and Problems of Water Percolation*; United States Bureau of Reclamation: Washington, DC, USA, 1953.